A CLEFT MODEL FOR CARDIAC PURKINJE STRANDS

DAVID N. LEVIN AND HARRY A. FOZZARD, *Department of Medicine and The Pharmacological and Physiological Sciences, University of Chicago, Chicago, Illinois 60637 U.S.A.*

ABSTRACT Conduction of the action potential in cardiac muscle is complicated by its multicellular structure, with narrow intercellular clefts and cell-to-cell coupling. A model is developed from anatomical data to describe cardiac Purkinje strands of variable diameter and different internal arrangements of cells. The admittance of the model is solved analytically and fit to results of cable analysis. Using the extracted specific membrane and cell electrical parameters (R_m = 13 $K\Omega cm^2$, C_m = 1.5 $\mu F/cm^2$, R_i = 100 Ωcm, and R_e = 50 Ωcm), the model correctly predicted conduction velocity and filling of capacitance at the onset of a voltage step. The analysis permits more complete studies of the factors controlling conduction velocity; for instance, the effect on conduction velocity of a capacity in the longitudinal current circuit is discussed. Predictions of the impedance and phase angle were also made. Measurements of the frequency dependence of phase angle may provide a basis for separating cleft membrane properties from those of the surface membrane and may aid the measurement of nonlinear membrane properties in muscle.

INTRODUCTION

The importance of complex morphology for the analysis of electrical properties of frog skeletal muscle was clearly shown by Falk and Fatt (1964), who proposed a two time-constant model and various distributed models for the surface and transverse tubular membranes. Similar characteristics in cardiac Purkinje fibers were shown by Fozzard (1966) and Freygang and Trautwein (1970). To describe charging of the transverse tubular system in skeletal muscle when potential across the external sarcolemma is changed, Adrian et al. (1969) proposed a disk model for the transverse tubules, which distributes tubular capacitance and conductance evenly in the fiber volume. This has been further refined from the original Falk and Fatt (1964) proposal into a mesh model more in keeping with the morphometry of skeletal muscle fibers by Mathias et al. (1977). The disk model of Adrian et al. (1969) fails to fit the passive cable properties of cardiac Purkinje strands (Schoenberg et al., 1975) and the geometry of the Purkinje strand is quite different from skeletal muscle (Mobley and Page, 1972; Hellam and Studt, 1974 *b*). In its place a cleft model has been proposed. This cleft model corresponded much more closely to the morphology of the cardiac Purkinje fiber, which is made up of several cells in cross section, closely packed together, so that most of the cell membranes face restricted extracellular spaces (Sommer and Johnson, 1968; Mobley and Page, 1972; Hellam and Studt, 1974 *a*). More complete mathematical development of the disk model for skeletal fibers by Adrian and Almers (1974) and Schneider and Chandler (1976) has permitted accurate measurement of transverse tubular capacitance and its changes with voltage. Complete passive analysis in the frequency domain for skeletal fibers has been greatly assisted by the disk model (Schneider, 1970; Valdiosera et al., 1974), and more morphometrically based models (Mathias et al., 1977). The success of this approach for skeletal muscle cells

suggests that a more thorough development of the cleft model for Purkinje strands would permit better understanding of conduction in the Purkinje strand (McAllister et al., 1975; Hunter et al., 1975) and better insight into the physiologic role of the intercellular clefts and their influence on voltage clamp studies (Schoenberg and Fozzard, 1979).

This article provides a development of the cardiac cleft model of the cable based on the measurable morphometric properties of the Purkinje strand. It leads to a general description of passive electrical properties in this tissue at the microscopic level, and emphasizes the critical importance of morphometry in such electrical studies. It also provides the opportunity to see how behavior of the cardiac strand differs from simple cables such as the squid axon or from frog skeletal fibers. Analytical equations are used to describe multicellular strands with diameters between 100 and 300 μm. The mathematical approaches of Hellam and Studt (1974 *b*) and Schoenberg et al. (1975) are extended to describe two different cell organizations, strands of larger diameters, and a larger range of conditions. The predictions of the analytical model are compared with previous experiments, especially those of Schoenberg et al. (1975) and Freygang and Trautwein (1970). Implications of the model for future experiments are developed for analysis of cable experiments, voltage clamps, impedance locus measurements, and studies of conduction under abnormal conditions.

SYMBOLS

The symbols used in this paper are listed in alphabetical order, first the Roman and then the Greek:

$\tilde{C}_{AP}$ apparent specific membrane capacitance (μF/cm^2) filled by the foot of the action potential; this is the value derived from the experimental data if we assume the strand is a smooth circular cylinder

C_m true unit membrane capacitance (μF/cm^2)

$\tilde{C}_m$ apparent specific membrane capacitance (μF/cm^2) filled by a step of injected current; this is the value deduced from experimental data when we ignore both the folding of external membrane and the existence of membrane facing clefts.

D fiber diameter (μm)

F the factor whose value (between zero and one) describes the effective decrease in internal membrane admittance due to the clefts; i.e., F gives the fraction of internal membrane which is effectively conducting.

I Laplace transform of the total current injected into the sealed ($x = 0$) end of a semi-infinite fiber.

k $1/\tau_{AP}$

L folded length (μm) of cell sides facing the intercellular clefts ($L = L_s\phi_i$)

L_c average circumferential distance (μm) between cleft mouths (folding ignored)

L_e, L_i total transverse lengths (μm) of membrane at the strand surface and membrane facing the clefts if folding is ignored.

p variable of Laplace transform with respect to time; the magnitude of p is $2\pi\nu$ where ν is frequency in Hz.

R_e specific resistivity of solution in clefts (Ωcm)

R_i specific resistivity of fiber interior (Ωcm)

r_i resistance per unit length (Ω/cm) of fiber interior

$\tilde{R}_i$, $\tilde{R}_m$ the naive or apparent value of R_i/R_m which would be derived from cable measurements of R_0 and Λ if the strand is assumed to be a smooth uninvaginated circular cylinder.

r_m surface membrane resistance ($K\Omega$cm) per unit length

R_m true unit membrane resistance ($K\Omega$cm^2)

U Laplace transformed potential (mV) in a cleft relative to zero bath potential

V Laplace transformed potential (mV) of fiber interior (relative to zero bath potential) minus the membrane resting potential (V_m)
w width (μm) of clefts
x distance along longitudinal axis of fiber (μm)
Y admittance (mS/cm^2) of a unit area of external or internal membrane
y_m effective admittance per unit length (S/cm) of whole fiber in the transverse direction
Z_x magnitude of the transfer impedance (kΩ) at position x; Z_0 is the characteristic impedance (kΩ)
θ velocity (m/s) of action potential
t_x magnitude of the phase of the transfer impedance at position x; θ_0 is the phase angle of the characteristic admittance
λ fiber length constant (mm); depends on Laplace transform variable p
Λ length constant (mm) of the steady state voltage distribution of a fiber
λ_c length constant (μm) for cleft voltage distribution in the transverse plane; depends on p.
ν frequency (Hz)
τ time constant (ms) of charging of a fiber after injection of a step of current
τ_{AP} time constant (ms) of foot of action potential
ϕ_e factors by which external and internal membrane lengths are increased by folding
ω angular frequency (s^{-1}) of alternating current: $\omega = 2\pi\nu$ where ν is frequency in Hz

THE MODEL

The Purkinje strand is represented by a bundle of cells with narrow intercellular clefts. The clefts are filled with electrolyte solution like Tyrode's solution, although it is not necessary for the conductance to be the same. The conductance and capacitance of the membranes lining the clefts may be different from those of the surface membranes. The cells are approximately the same size so that larger strands are simply composed of more cells. The cells may have irregular shapes; for instance, the membranes may have folds, increasing their surface area above that calculated on the basis of a smooth membrane envelope. The folding factors need not be the same for the surface and for the clefts. The cells are well coupled electrically in both planes, but there is a possibility of capacitive coupling at the intercalated disks.

The equations to be solved require a detailed description of the internal morphology of the Purkinje strand. This was based on the morphometric work of Mobley and Page (1972) and Hellam and Studt (1974 *a*). The intercellular clefts are assumed to have an average width (w) of 0.04 μm, and to meander with a periodicity greater than w. The meandering of the membrane is described by folding factors, $\phi_i = 1.9$ (cleft membrane) and $\phi_e = 1.4$ (surface membrane). Transverse and longitudinal folding factors are assumed to be the same for simplicity, but the equations permit introduction of differences. In a transverse section the cells have a uniform cross section if folding is ignored (Fig. 1). Since real strands would have a variable number of cells meeting at cleft junctions, we consider the cases of three clefts (hexagonal cells) and six clefts (triangular cells) meeting at each junction. The two cases should represent the extremes, with the real strand having an intermediate structure. The pairs of models in Fig. 1 have cells of the size to keep the overall strand cross sectional areas equal to $\pi D^2/4$, where D is strand diameter. The membranes are presumed to be folded, and the cells may have deformed shapes, as in Fig. 2. In this model comparison of the influence of diameter and convergence of clefts, the paired models have the same diameter, but different amounts of membrane. The effect of this different membrane area can be separated from that of the convergence by altering the folding factors to equalize the membrane areas.

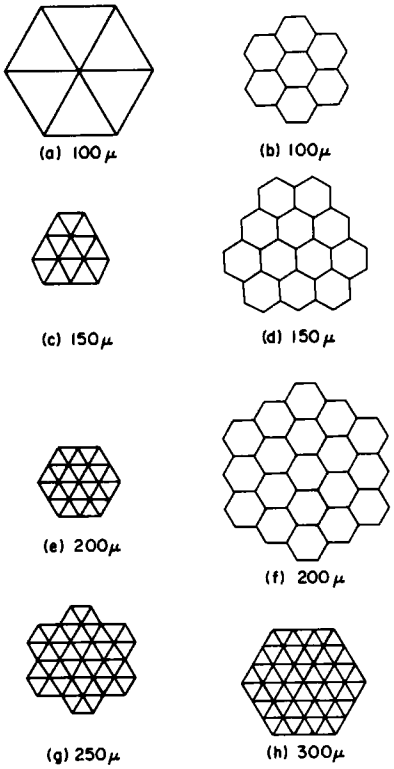

FIGURE 1 Purkinje fiber models seen in transverse section and labeled by the diameter (D) of the corresponding circular cylindrical fiber. The scale of each model (i.e., the length of each cell side) is chosen so that the cross-sectional area is $\pi D^2/4$. Note that these diagrams are a shorthand notation for folded, deformed models like the one illustrated in Fig. 2 *c*.

There are four electrical approximations used in the mathematical analysis:

(*a*) There is no voltage variation in the transverse plane. This assumes one-dimensional current flow inside the strand. Eisenberg and Johnson (1970) have discussed corrections to be expected from three-dimensional effects in cells without clefts. They point out that the transverse voltage gradient is significant if the cell membranes are leaky enough, and some gradient would always be seen sufficiently close to the diverging current near a current-passing electrode. Estimates of the importance of the three-dimensional effect in our models indicate that it is <0.05 up to 10^4 Hz, if the recording electrode is >1 strand diameter distant

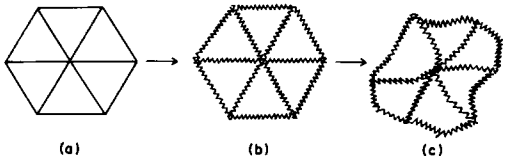

FIGURE 2 The pictures in Fig. 1 (e.g., *a*) are schematic representations of models which have folded internal and external membrane (*b*). Also, the analytic results in this paper continue to hold even if a model is deformed (*c*) in any way which does not change the area or average side lengths.

from the current-passing electrode. Fozzard and Schoenberg (1973) were not able to identify experimentally a three-dimensional effect up to $\sim 10^3$ Hz, at a distance of ~ 1 diameter from the current passing electrode. However, this has not been examined as carefully in cardiac fibers as it has in skeletal muscle (Valdiosera et al., 1974).

(*b*) The flow of cleft current in the longitudinal direction is assumed to be much smaller than the flow in the transverse direction. The ratio of longitudinal to transverse cleft currents can be approximated by the ratio of voltage gradients, which is described by $\lambda_c/\lambda\phi_i$, where λ_c is the cleft length constant and λ is the strand's longitudinal length constant. Estimates of λ_c by Schoenberg et al. (1975) and Hellam and Studt (1974 *b*) show this ratio to be <0.06 up to 10^4 Hz. Analog simulation by Hellam and Studt (1974 *b*) suggested an even smaller longitudinal current flow in the clefts. It is further assumed that the variation of voltage across the cleft width is small. An estimate with typical parameters suggests that this variation is $<10^{-5}$.

(*c*) The surface and cleft membranes are assumed to have the specific admittance (Y) of a parallel resistor and capacitor:

$$Y = \frac{1}{R_m} + C_m p, \tag{1}$$

where R_m is the unit membrane resistance, C_m is the unit membrane capacitance, and p is the Laplace transform variable (the absolute magnitude of p is $2\pi\upsilon$, where υ is frequency in Hz). The initial derivation will assume that the surface and cleft membranes have the same Y. This assumption is not essential, and the modifications for different Y will be made later.

(*d*) The strand interior is first assumed to be purely resistive, with a specific resistivity R_i. For the cytoplasm this is a reasonable assumption. However, the cells are coupled at intercalated disks, where two membranes are separated by a narrow space. Freygang and Trautwein (1970) found a capacitive element encountered by longitudinal currents in the Purkinje strand, with a time constant of 64 μs. After development of the simpler model, the effect of such a capacitive element will be examined.

CALCULATION OF ADMITTANCE

Strands of the sort described can be represented by the circuit in Fig. 3, longitudinal intracellular current being related to an effective resistance per unit length (r_i) and the

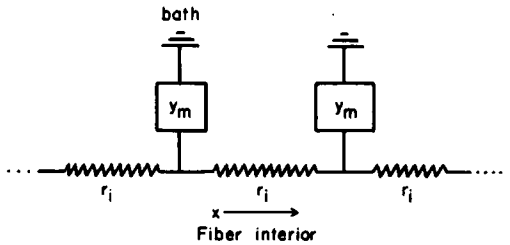

FIGURE 3 The cable circuit representing any fiber which is subject to the electrical approximations *a*, *b*, *c*, and *d* in the text. The elements r_i and y_m denote the internal resistance and effective admittance per unit length.

transverse current flow being related to effective admittance per unit length (y_m). Therefore,

$$V = Ir_i\lambda e^{-x/\lambda}$$

$$r_i = 4R_i/\pi D^2$$

$$\lambda = \sqrt{\frac{1}{r_i y_m}}. \tag{2}$$

Here λ is the longitudinal length constant, I is the Laplace transform of the total current injected at a sealed end ($x = 0$), and V is the Laplace transformed potential of the strand interior minus the membrane resting voltage. Note that I, y_m, and λ depend on the Laplace variable p. Let L_e and L_i denote the lengths of surface and cleft membrane in the transverse plane if folding is ignored. The actual lengths are then $L_e\phi_e$ and $L_i\phi_i$. y_m is the admittance per unit length of strand, and it is therefore the sum of the admittances of the surface membrane and the cleft membrane.

$$y_m = Y(L_e\phi_e^2 + L_i\phi_i^2 F). \tag{3}$$

The amount of additional admittance resulting from the presence of clefts varies with the factor F, which is 1 if there is no voltage decrement in the clefts and 0 if the cleft membrane is completely inaccessible. F, therefore, describes the effective fraction of cleft membrane that conducts current.

Since cleft current flows parallel to the cleft membranes in the transverse plane, the cleft voltage distribution will obey a cable equation (Schoenberg et al., 1975) in which the cleft length constant is

$$\lambda_c = \sqrt{\frac{w}{2R_e Y}}, \tag{4}$$

where R_e is the specific resistivity of the fluid in the cleft. The specific admittance for cleft membrane is assumed here to be the same as that of the surface membrane. λ_c represents the decrement in voltage along the length of the cleft, which meanders according to the folding factor ϕ_i. This differs from the definition of Schoenberg et al. (1975), so that λ_c (this definition) = $\phi_i\lambda_c$ (Schoenberg et al., 1975). The definition used here can be more conveniently related to morphometric values.

The factors F and y_m can be determined from the exact geometrical conditions illustrated in Fig. 1. To find y_m it is sufficient to consider the intracellular compartment to be space-clamped at the voltage V. Then y_m is the leakage current per unit length divided by V. The current leaking through the surface membrane is $L_e\phi_e^2 YV$. The current leaking out through the cleft membrane is the total current leaking out of cleft mouths at the surface. It can be described by a method similar to that used by Schoenberg et al. (1975) and Mathias et al. (1977). Let U be the Laplace-transformed voltage in any cleft relative to the bath and ℓ be the distance along the cleft in the transverse plane. Let $dU_{mouth}/d\ell$ denote the derivative of the cleft voltage just inside a cleft mouth; the derivative is taken in the direction pointing out of the cleft. This is the electric field in the inward direction. Therefore, the current leaking out through a unit length of cleft mouth is $-w\phi_i/R_e\, dU_{mouth}/d\ell$ since $1/R_e$ is the conductivity in

the cleft and $w\phi_i$ is the area of a unit length of cleft mouth. Therefore,

$$y_m = L_e\phi_e^2 Y - \frac{w\phi_i}{R_e V} \sum_{\substack{\text{cleft} \\ \text{mouths}}} \frac{dU_{\text{mouth}}}{d\ell}. \tag{5}$$

To find $dU/d\ell$ at each cleft mouth, it is necessary to find the voltage distribution along each cleft. At any value of ℓ the current flowing down a unit length of cleft is $-w\phi_i/R_e\, dU/d\ell$. The current leaking into a unit length of cleft of unit depth is exactly $2\phi_i Y(V - U)$. Since this must be the rate of change of cleft current with respect to ℓ,

$$\frac{d}{d\ell}\left[\frac{-w\phi_i}{R_e}\frac{dU}{d\ell}\right] = 2\,\phi_i Y\,(V - U),$$

or

$$\frac{d^2}{d^2\ell}(V - U) = (V - U)/\lambda_c^2, \tag{6}$$

where

$$\lambda_c = \sqrt{\frac{w}{2R_e Y}}.$$

Therefore, $V - U$ satisfies a cable equation with a length constant of λ_c. The general solution has the form

$$V - U = A\cosh(\ell/\lambda_c) + B\sinh(\ell/\lambda_c), \tag{7}$$

where A and B are determined by the values of U (call them U_+ and U_-) at the cleft ends. Let $dU_+/d\ell(dU_-/d\ell)$ be the derivative evaluated at the $+(-)$ end, going out of a cleft to a junction or the bath. Rearrangement of Eq. 7 implies

$$\frac{dU_+}{d\ell} = \frac{-1}{\lambda_c}\left[\frac{U_-}{\sinh(L/\lambda_c)} - U_+\coth(L/\lambda_c) + V\tanh(L/2\lambda_c)\right], \tag{8}$$

where L is the folded length of cleft membrane on one side of a cell.

Consider the special case in which the cleft is terminated at the surface of the strand. Let $U_+ = U_{\text{mouth}}$ be the potential (equal to zero) at the cleft mouth and let $U_- = U_{\text{inner}}$ be the potential at the "inner" end of the cleft. Substituting Eq. 8 into Eq. 5 gives

$$y_m = L_e\phi_e^2 Y + 2N_c\phi_i Y\lambda_c\tanh(L/2\lambda_c) + \frac{2\phi_i Y\lambda_c}{V\sinh(L/\lambda_c)} \sum_{\substack{\text{superficial} \\ \text{clefts}}} U_{\text{inner}}, \tag{9}$$

where N_c is the number of cleft mouths at the surface.

y_m is determined by the potentials at the inner ends of the superficially located clefts; these potentials can be found by solving algebraic equations obtained by requiring conservation of current at each junction. Label each junction in the strand with the index integer k, and let N_k be the number of cleft ends forming the k^{th} junction. For each cleft at the k^{th} junction, let $(+)$ label the end joining the junction and $(-)$, the opposite end. Current conservation requires

that the sum of all currents flowing into the k^{th} junction be zero; therefore,

$$\frac{-w\phi_i}{R_e} \sum_{\substack{\text{clefts at} \\ \text{junction } k}} \frac{dU_+}{d\ell} = 0. \tag{10}$$

Cancelling the common factor and substituting Eq. 8 implies

$$N_k U_+ \cosh(L/\lambda_c) - \sum_{\substack{\text{clefts at} \\ \text{junction } k}} U_- = N_k V \sinh(L/\lambda_c) \tanh(L/2\lambda_c), \tag{11}$$

where U_+ denotes the potential at the k^{th} junction and the U_-s denote potentials at the cleft ends one length away from k. Note U_- is zero for clefts that connect k to the surface. Eq. 11 and analogous equations for all other junctions form a set of simultaneous algebraic equations that can be solved for U at every junction. After this is done, y_m is found by substituting U at superficial junctions into Eq. 9.

These results have a simpler appearance if the quantity $[V \sinh(L/\lambda_c) \tanh(L/2\lambda_c)]$ is factored out, i.e., let U be the potential at some junction and define S at that junction to be

$$S = \frac{U}{V \sinh(L/\lambda_c) \tanh(L/2\lambda_c)}. \tag{12}$$

Rewriting Eq. 11 in terms of S,

$$S_+ \cosh(L/\lambda_c) - \frac{1}{N_k} \sum_{\substack{\text{clefts at} \\ \text{junction } k}} S_- = 1. \tag{13}$$

Let N_i be the number of cleft cell sides in any transverse section; $N_i = L_i\phi_i/L$. This and Eq. 12 can be used to rewrite Eq. 9 as

$$y_m = Y(L_e\phi_e^2 + L_i\phi_i^2 F), \tag{14a}$$

where

$$F = G \frac{\tanh(L/2\lambda_c)}{(L/2\lambda_c)}, \tag{14b}$$

$$G = \frac{1}{N_i}\left(N_c + \sum_{\substack{\text{superficial} \\ \text{clefts}}} S_{\text{inner}}\right) \tag{14c}$$

Eqs. 13 and 14 can be used to find the admittance of any model in Fig. 1 in the following way: (*a*) Write Eq. 13 for each junction, using S_+ for the S value at that junction and S_- for the S values at the cleft ends that are one cleft length away. (*b*) Solve the resulting system of linear equations for S by calculating the determinants in Cramer's rule. (*c*) Substitute values of S at superficial junctions into Eq. 14c. Then Eqs. 14a and 14b specify the admittance of that model in terms of its geometric and electrical parameters. The results of such calculations are given in Table I.

Consider the example of the 24 triangle model of a 200-μm strand (Fig. 1 *e*). Symmetric models of this type are particularly simple. All superficial junctions have the same value S_1. The central junction has some other value S_2. Writing Eq. 13 at the superficial and central

TABLE I
ADMITTANCES OF MODELS *a–h* OF FIG. 1

Model	Cell No.	Diameter	L_s	L_i/L_e	G
		(μm)	*(μm)*		
1*a*	6	100	55	2	$\frac{H+1}{2H}$
1*b*	7	100	21	4/3	$\frac{3H+1}{4(3H-2)}$
1*c*	13	150	56	10/3	$\frac{2(3H+2)}{5(3H-1)}$
1*d*	12	150	24	2	$\frac{81H^4+81H^3-9H^2-21H-4}{16(27H^4-21H^2+2)}$
1*e*	24	200	55	5	$\frac{3H(3H+2)}{5(6H^2-2H-1)}$
1*f*	19	200	25	14/5	$\frac{27H^3-12H-1}{7(27H^3-27H^2-3H+5)}$
1*g*	42	250	52	6	$\frac{45H^3+30H^2-8H-4}{9(18H^3-6H^2-5H)}$
1*h*	54	300	55	8	$\frac{180H^4+120H^3-33H^2-31H-4}{8(108H^4-36H^3-45H^2+2)}$

Determined by using the geometry-dependent function G in Eqs. 14a and 14b. L_s refers to the length of each cell side with folding ignored; L_i/L_e designates the ratio of the transverse length of internal and external membrane with folding ignored. H stands for $\cosh(L/\lambda_c)$.

junctions yields

$$S_1 \cosh(L/\lambda_c) - \frac{1}{6}(2S_1 + S_2) = 1$$

$$S_2 \cosh(L/\lambda_c) - \frac{1}{6}(6S_1) = 1. \tag{15}$$

Cramer's rule gives the solution for S_1:

$$S_1 = \begin{vmatrix} 6 & -1 \\ 1 & \cosh(L/\lambda_c) \end{vmatrix} \Big/ \begin{vmatrix} -2 + 6\cosh(L/\lambda_c) & -1 \\ -1 & \cosh(L/\lambda_c) \end{vmatrix} \tag{16}$$

or

$$S_1 = \frac{6\cosh(L/\lambda_c) + 1}{6\cosh^2(L/\lambda_c) - 2\cosh(L/\lambda_c) - 1}$$

Substituting Eq. 16 into Eq. 14c gives the result in Table I:

$$G = \frac{3H(3H+2)}{5(6H^2-2H-1)}, \tag{17}$$

where $H = \cosh(L/\lambda_c)$. Now Eq. 17, 14b, and 14a completely specify the admittance of the model in Fig. 1 *e*.

The above results can be used to derive a universal high frequency form of y_m for any strand made up of cells whose cleft sides have a folded length equal to L. As frequency increases, Y grows, λ_c becomes much smaller than L, and $\cosh(L/\lambda_c)$ becomes large. Therefore, Eq. 13 indicates that

$$S \to \frac{1}{\cosh(L/\lambda_c)} \tag{18}$$

Here we have dropped terms of order $1/\cosh^2(L/\lambda_c)$ or equivalently of order e^{-2L/λ_c}. Eq. 18 states that all junctions are at nearly equal potentials; this is reasonable since little current flows through the deep clefts when $\lambda_c \ll L$. Substituting Eq. 18 into Eq. 14c shows that

$$G \to \frac{N_c}{N_i}\left(1 + \frac{1}{\cosh(L/\lambda_c)}\right). \tag{19}$$

Here we have assumed that the inner end of each superficial cleft reaches a junction. Since the factor in parentheses is equal to $1/\tanh(L/2\lambda_c)$ up to terms of order e^{-2L/λ_c}, Eq. 19 can be written as

$$G \to \frac{N_c}{N_i \tanh(L/2\lambda_c)}. \tag{20}$$

Now, Eq. 14b shows the high frequency limit of F:

$$F \to \frac{2N_c\lambda_c}{N_iL}. \tag{21}$$

Substituting Eq. 1 into the expression for λ_c (Eq. 6) gives

$$\lambda_c = \left[\frac{w}{2R_eC_mp\left(1 + \frac{1}{R_mC_mp}\right)}\right]^{1/2}.$$

If we ignore terms of order $1/R_mC_mp$:

$$\lambda_c \to \sqrt{\frac{w}{2R_eC_mp}}$$

and

$$F \to \frac{N_c}{N_iL}\sqrt{\frac{2w}{R_eC_mp}}. \tag{22}$$

Therefore, Eq. 3 shows that the high frequency form of y_m is

$$y_m \to L_e\phi_e^2Y\left[1 + \frac{\phi_i}{\phi_e^2L_c}\sqrt{\frac{2w}{R_eC_mp}}\right], \tag{23}$$

where L_c is the average spacing ($= L_e/N_c = \pi D/N_c$) between cleft mouths at the surface. Eq. 23 can be applied at the frequency associated with the foot of the action potential, $p \simeq 1/\tau_{AP}$, since correction terms of order e^{-2L/λ_c} and $1/R_mC_mp$ are very small (<1%) for reasonable values of the electrical parameters.

RESULTS

The equations for admittance in the cable with clefts are based on idealized anatomical characteristics. Adaptations of these equations will now be used for comparison with experimental electrophysiological studies. The first question is comparison between the six-junction (triangle) models and the three-junction (hexagon) models. The influence of this internal geometry should be most apparent in strands of large dimension and during studies at low and intermediate frequencies. Therefore, the equations will be used to predict the results of standard (d.c.) cable analysis and the measurements made during action potential propagation. The second question is comparison between behavior at low frequency and that at high frequency. Data extracted from cable analysis will be used to predict measurements made during propagated action potentials and during voltage steps. Finally, the full range of linear electrical behavior will be examined by comparing predictions of these models with phase angle and impedance studies. In some cases data that fully exercise the model are not available, so that model predictions are made for future experimental consideration.

Cable Analysis

In standard cable analysis (Weidmann, 1952; Fozzard, 1966) the basic measurements are input residence (R_o), length constant (Λ), and time constant (τ). From these are derived the unit membrane resistance (R_m), the unit membrane capacitance (C_m), and the core resistance per unit length (r_i). It is apparent from Eqs. 2 and 3 that R_o and Λ are related to the value of the frequency-dependent length constant $\lambda\,(p)$ at $p = 0$ (d.c. conditions):

$$R_0 = r_i\lambda(0)$$

$$\Lambda = \lambda(0) = \left[\frac{r_m}{r_i\left(1 + \dfrac{L_i\phi_i^2}{L_e\phi_e^2}F(0)\right)}\right]^{1/2} \tag{24}$$

where r_m is the external membrane resistance of a unit length ($R_m/L_e\phi_e^2$). The value of F at $p = 0$ is given by Eq. 14b and Table I. In cable analysis the specific cell properties are calculated in terms of the measured parameters:

$$\tilde{R}_i = \pi D^2 R_0/4\Lambda$$

$$\tilde{R}_m = \pi D R_0 \Lambda$$

$$\tilde{C}_m = \frac{\tau}{\pi D R_0 \Lambda}, \tag{25}$$

where $\tau = R_m\,C_m$ is the membrane time constant of a strand. Hodgkin and Rushton (1946) showed that the charging of a fiber without clefts is described by an error function

characterized by the time constant $R_m C_m$. The charging of a Purkinje strand will deviate from the Hodgkin-Rushton formula at times which are comparable to the time constant associated with the cleft spaces (usually a few milliseconds). This deviation has been measured experimentally (Fozzard, 1966) and has been calculated analytically (Levin and Fozzard, unpublished observations). At much larger times, Purkinje strand charging is described by the Hodgkin-Rushton error function formula with an accuracy better than 5%. Therefore, the membrane time constant can be measured by the usual method of fitting the charging curve at large times to the Hodgkin-Rushton formula. The quantities $\tilde{R}_i$, $\tilde{R}_m$, and $\tilde{C}_m$ represent the apparent internal resistivity, membrane resistivity, and capacitance seen by a step of injected current, referred to a smooth circular cylinder of diameter D. Substituting the relationships in Eq. 24 gives the apparent electrical parameters in terms of the true properties:

$$\tilde{R}_i = R_i \tag{26a}$$

$$\tilde{R}_m = \frac{R_m}{\phi_e^2\left[1 + \frac{L_i\phi_i^2}{L_e\phi_e^2} F(0)\right]} \tag{26b}$$

$$\tilde{C}_m = C_m\phi_e^2\left[1 + \frac{L_i\phi_i^2}{L_e\phi_e^2} F(0)\right]. \tag{26c}$$

These equations can be used to compare the two types of models with experimental data of Schoenberg et al. (1975). Those experiments were performed in Tyrode solution with a specific resistivity of ~50 Ωcm. Eq. 26a shows that the usual formula for R_i (Hodgkin and Rushton, 1946) is not modified by the presence of clefts. Therefore, the cable data of Schoenberg et al. (1975) implies that $R_i \simeq 100$ Ωcm, as reported in that paper. It is hard to say how this core resistivity should be distributed between the myoplasm and gap junctions. The data on apparent membrane resistivity and capacity were compared with the predictions of Eqs. 26b and 26c. The calculations were made with F from Eq. 14b and Table I, with geometrical parameters of $w = 0.04$ μm, $\phi_e = 1.4$, and $\phi_i = 1.9$, and with electrical parameters of $R_m = 13$ kΩcm^2, $C_m = 1.5$ μF/cm^2, and $R_e = 50$ Ωcm (Figs. 4 and 5). Predictions made with $R_e = 450$ Ωcm are also shown. Both models show a rise in $1/\tilde{R}_m$ and $\tilde{C}_m$ with increased diameter. The increase with diameter was better fit with the triangular cell model, but this was largely a consequence of the difference in membrane area in the two types of model. Calculations of $\tilde{C}_m$ and $1/\tilde{R}_m$ with the inner cleft membrane area of the hexagonal model made equal to that of the triangular model resulted in values within 5% of the triangular model predictions for each diameter. Consequently, almost all of the difference in the model predictions seen in Figs. 4 and 5 is produced by the area difference, and not by the number of clefts converging. It seems likely that the Purkinje strand would fall between these two models. Calculations with higher R_e in both models gave a poor fit, consistent with the idea that free diffusion of Tyrode solution occurs in the clefts. Calculations with systematic variation in R_m and C_m showed that the data could not be fit outside the limits $R_m = 16 \pm 8$ kΩcm^2 and $C_m = 1.50 \pm 0.7$ μF/cm^2, similar to the estimates of Schoenberg et al. (1975). This sort of experiment gives little additional information.

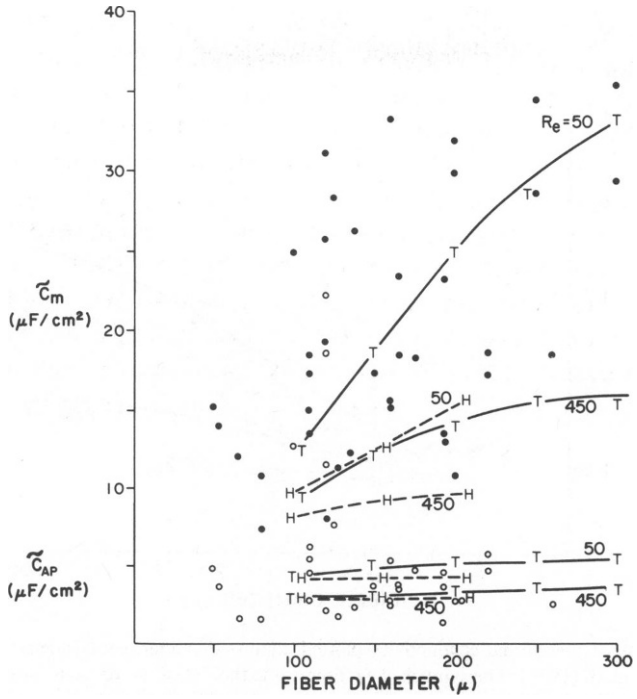

FIGURE 4 Apparent membrane capacity filled by a step of injected current and apparent capacity filled by the foot of the action potential plotted against diameter. The experimental points for $\tilde{C}_m$ (solid dots) and $\tilde{C}_{AP}$ (open circles) are taken from Schoenberg et al. (1975). The symbols T (H) mark the theoretical predictions for the triangular-cell (hexagonal-cell) models in Fig. 1. These predictions are obtained by using R_m = 13 kΩcm^2, C_m = 1.5 μF/cm^2, $k^{-1} = \tau_{AP}$ = 0.1 ms, and R_e = 50 or 450 Ωcm in the right side of Eqs. 26c and 28. Solid (dashed) lines are drawn through the triangular-cell (hexagonal-cell) points to guide the eye.

Conduction Velocity and Capacity of the Action Potential Foot

The time constant of the propagating action potential foot (τ_{AP}) and conduction velocity (Θ) are related to the passive cable properties by the Tasaki-Hagiwara equation (1957).

$$\theta^2 = \frac{D}{4R_i \tilde{C}_{AP} \tau_{AP}} \tag{27}$$

where $\tilde{C}_{AP}$ is the apparent membrane capacity filled by the foot of the action potential. It is easy to show that the wave equation for an action potential and Eq. 2 imply that the time constant of the foot satisfies $\theta = k\lambda$ (k), where $k = 1/\tau_{AP}$. The connection between $\tilde{C}_{AP}$ and C_m in any model is easily derived by combining the above relationship with Eqs. 27, 2, and 3:

$$\tilde{C}_{AP} = C_m \phi_e^2 \left[1 + \frac{L_i \phi_i^2}{L_e \phi_e^2} F(k)\right]. \tag{28}$$

When we substitute values of R_m and C_m deduced from the d.c. analysis into Eq. 28, we are led to predict values of $\tilde{C}_{AP}$ which agree with experiment as shown in Fig. 4. Notice that the

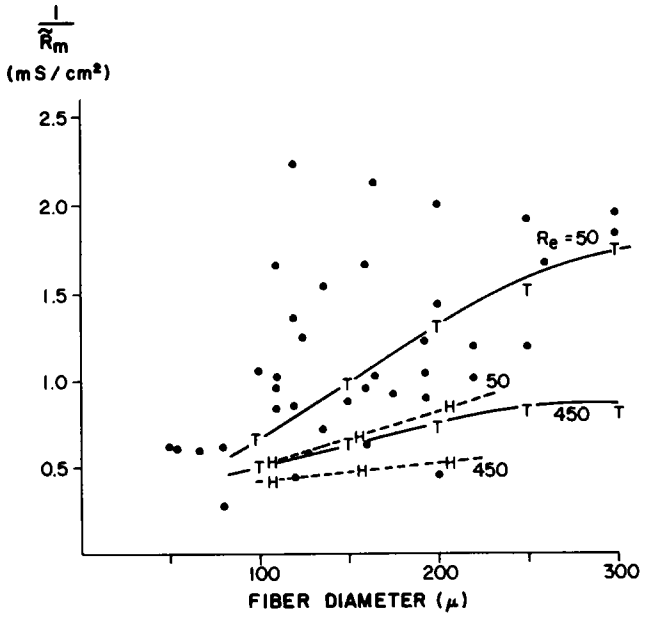

FIGURE 5 Apparent membrane conductivity plotted against diameter; experimental points are taken from Schoenberg et al. (1975). The symbols T (H) mark the theoretical predictions for the triangular-cell (hexagonal-cell) models in Fig. 1. These predictions are obtained by substituting R_m = 13 kΩcm², C_m = 1.5 μF/cm², and R_e = 50 or 450 Ωcm into the right side of Eq. 26b. The solid (dashed) lines are drawn through the triangular-cell (hexagonal-cell) predictions to guide the eye.

triangular and hexagonal cell models are almost identical, since at the frequency of the normal Purkinje strand action potential ($1/2\pi\tau_{AP}$ = 1,600 Hz) the measurement of capacitance is dominated by the surface membrane and the cleft mouths. This can be made mathematically explicit by noticing that the large value of k allows us to approximate the bracketed factor in Eq. 28 by the bracketed factor in Eq. 23:

$$\tilde{C}_{AP} = C_m\phi_e^2\left(1 + \frac{\phi_i}{\phi_e^2 L_c}\sqrt{\frac{2w}{R_e C_m k}}\right). \tag{29}$$

Inserting the standard values into this equation (but adopting the suggestion of Schoenberg et al. [1975] that ϕ_i at the mouth is the same as ϕ_e) results in $\tilde{C}_{AP}$ = 4.2 μF/cm², close to the experimental result. Note that this formula does not contain any descriptors of the strand's internal architecture, and it does not depend on geometrical details as long as $L \gg \lambda_c(k)$. It also shows that $\tilde{C}_{AP}$ is independent of diameter, in agreement with the experimental results shown in Fig. 4.

The relatively model-independent equation for $\tilde{C}_{AP}$ (Eq. 29) can be inserted into the Tasaki-Hagiwara equation (Eq. 27) to describe θ.

$$\theta^2 = \frac{kD}{4R_i C_m \phi_e^2\left(1 + \frac{\phi_i}{L_c\phi_e^2}\sqrt{\frac{2w}{R_e C_m k}}\right)}. \tag{30}$$

The familiar dependency of θ on $D^{1/2}$ is not altered by the clefts. Since the advancing foot depolarizes only the cleft mouths, the different amount of cleft membrane in larger fibers does not influence θ, as long as the average distance between cleft mouths is the same. Evaluation of this relationship requires knowledge of R_e in the clefts. It is reasonable to use the value of R_e in the bathing solution because depolarization reaches into the clefts only ~10 μm, where exchange with Tyrode solution should be good. When the values of C_m and R_i extracted from the d.c. analysis are used in Eq. 30, we predict that θ is 2.8 m/s for a 150-μm strand, compared to the experimental average of 3.0 m/s (Schoenberg et al, 1975).

The observation of Freygang and Trautwein (1970) of a capacitive element for current flowing longitudinally in the strand interior would influence the calculation of $\tilde{C}_{AP}$ and θ. To estimate the importance of this factor we need to replace R_i with Z_i, the specific impedance of the core. This can be written $Z_i = R_i\gamma(p)$, where γ is a frequency-dependent factor equal to unity at $p = 0$. Eqs. 29 and 30 become

$$\tilde{C}_{AP} = C_m\phi_e^2\gamma(k)\left(1 + \frac{\phi_i}{L_c\phi_e^2}\sqrt{\frac{2w}{R_eC_mk}}\right) \tag{31}$$

$$\theta^2 = \frac{kD}{4R_iC_m\phi_e^2\gamma(k)\left(1 + \frac{\phi_i}{L_c\phi_e^2}\sqrt{\frac{2w}{R_eC_mk}}\right)} \tag{32}$$

If the core impedance is composed of a myoplasmic resistance (R_{i1}) in series with a parallel array of a second resistance (R_{i2}) and a capacitance (C_i), then Z_i is given by

$$R_i = R_{i1} + R_{i2}$$

$$\gamma(p) = \frac{1 + \frac{R_{i1}R_{i2}C_ip}{R_{i1} + R_{i2}}}{1 + R_{i2}C_ip}. \tag{33}$$

Using data from Table VIII of Freygang and Trautwein (1970) and τ_{AP} = 0.1 ms, we can calculate $\gamma(k)$ to be 0.936. Introducing this factor into the calculation of θ results in a value of 2.9 m/s, somewhat closer to the value of Schoenberg et al. (1975), but with a change of only 3%.

Eq. 30, which relates passive properties and cleft geometry to conduction, could be tested experimentally. θ and k could be reduced by replacing part of the Na^+ in the bath with an impermeant cation, or with tetrodotoxin. Change in R_e would be unlikely to provide a useful test because its role is small. However, R_i might be changed by an increase in intracellular Ca^{++} (DeMello, 1975; Weingart, 1977). Geometrical alterations would also be of great interest, but the need to perform morphometric analysis makes this approach difficult.

It is possible to provide a guide to experimental cable analysis that reduces the complexity introduced by clefts, so that extracted membrane values depend only on the accuracy of the morphometric characteristics of the strands. Eq. 29 can be rewritten as

$$\frac{\tilde{C}_{AP}}{\tau_{AP}} = \phi_e^2\left(\frac{C_m}{\tau_{AP}}\right) + \frac{\phi_i}{L_c}\sqrt{\frac{2w}{R_e}\cdot\frac{C_m}{\tau_{AP}}}. \tag{34}$$

R_e is assumed to be the resistivity of the Tyrode's solution, since the second term on the righthand side represents the effect of only ~10 μm of cleft membrane in the mouths and since Eq. 34 is only weakly dependent on the value of R_e (the second term is smaller than the first and R_e appears as the square root). If we take the previously used values of $L_c = 50$ μm, $\phi_e = 1.4$, $\phi_i = 1.9$, and $w = 0.04$ μm, we obtain

$$\frac{\tilde{C}_{AP}}{\tau_{AP}} = 1.96\left(\frac{C_m}{\tau_{AP}}\right) + 4.62\left(\frac{C_m}{\tau_{AP}}\right)^{1/2}. \tag{35}$$

Fig. 6 shows the plot of $\tilde{C}_{AP}/\tau_{AP}$ against C_m/τ_{AP}. Cleft effects (the second term on the right in Eq. 35) cause the curve to diverge from the dotted line, which represents the surface membrane of the strand (first term). The graph makes it easy to use experimental values of $\tilde{C}_{AP}$ and τ_{AP} to find C_m for any given strand. Using Eq. 35 and $\tau = R_m C_m$ to calculate R_m and C_m for each strand measured by Schoenberg et al. (1975) and plotting these values against diameter showed the disappearance of the apparent diameter dependence encountered in Figs. 4 and 5. It was found that the membrane parameters of single strands, which were calculated in this way, clustered near the values: $R_m \simeq 16$ kΩcm^2 and $C_m \simeq 1.4$ μF/cm^2. While these average results are reasonable, experiments designed to measure more carefully the necessary electrical and geometrical parameters would be desirable.

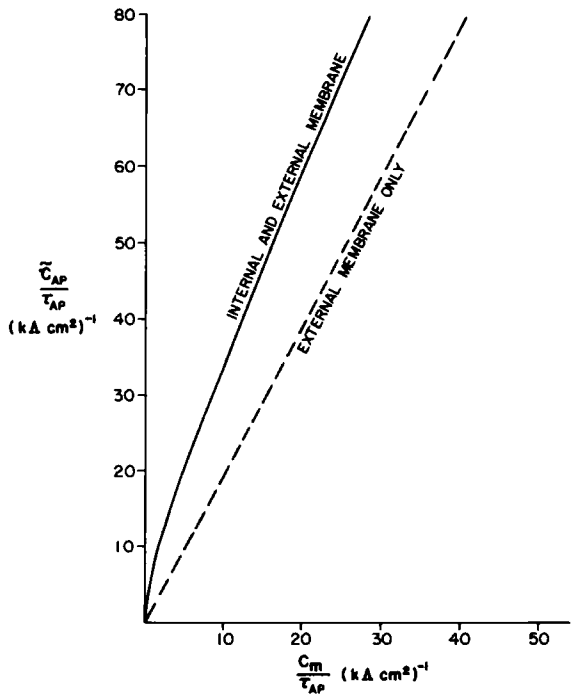

FIGURE 6 The relationship (solid line) between $\tilde{C}_{AP}/\tau_{AP}$ and C_m/τ_{AP} for a fiber of arbitrary diameter and cell composition. This line represents the sum of the first (external membrane) and second (internal membrane) terms in Eqs. 34 or 35. The dotted line represents the contribution of external membrane only.

Voltage Step

Another experiment that has given useful data is the voltage step applied to a very short strand. Fozzard (1966) found that the capacitive charging of the membrane appeared to occur in two phases, with a second charging time constant of ~2 ms. To compare these data with the cleft model, it is convenient to rephrase the admittance equations as follows. Eq. 14b and Table I provide a closed description of F for each model in Fig. 1. Complex analysis shows that the function F is analytic (except for poles labeled Y_n) despite the presence of square roots of functions of p. Cauchy's theorem can be used to put F into the form:

$$F = \sum_n \frac{(\text{residue of } F \text{ at } Y_n)}{Y - Y_n}. \tag{36}$$

For example, for the pie model of Fig. 1 *a* calculation shows that the poles are located at $Y_n = -n^2\pi^2 w/8L^2R_e$ (n = odd ≥ 1) and that the residue at each pole is w/L^2R_e. Using this in Eq. 36 and substituting the result in Eq. 3 gives

$$y_m = L_e\phi_e^2 Y + \sum_{n=\text{odd}\geq 1} L_{in}\phi_i^2 \frac{Y}{1 + R_{sn}Y},$$

where

$$R_{sn} = \frac{8L^2R_e}{n^2\pi^2 w} \tag{37}$$

and

$$L_{in} = \frac{8L_i}{n^2\pi^2}.$$

This form of y_m is mathematically equivalent to the closed form developed before. In the Appendix, Eq. 37 is shown to imply that the pie model is electrically equivalent to a specific distributed circuit (Fig. 12) in which cleft membrane is represented as an array of laminated membrane segments.

Suppose that a very short strand is space-clamped and that the voltage is stepped from zero to V_s at $t = 0$. Then the Laplace-transformed voltage is V_s/p. Let $J(p)$ be the Laplace transform of the resulting current per unit length of fiber. Then,

$$J(p) = \frac{y_m V_s}{p}. \tag{38}$$

Substituting Eq. 37 and inverting the Laplace transform gives

$$\frac{J(t)}{V_s} = L_e\phi_e^2 C_m\delta(t) + \frac{L_e\phi_e^2}{R_m} + \sum_{n=\text{odd}\geq 1} L_{in}\phi_i^2\left[\frac{1}{R_{sn} + R_m} + \frac{R_m}{R_{sn}(R_{sn} + R_m)} e^{-t/\tau_n}\right], \tag{39}$$

where

$$\tau_n = \frac{C_m}{\dfrac{1}{R_m} + \dfrac{1}{R_{sn}}}.$$

The symbol $\delta(t)$ denotes a spike with unit area so that $L_e\phi_e^2 C_m\delta(t)$ represents the rapid charging of the surface membrane capacity. The next term, $L_e\phi_e^2/R_m$, is the current through the surface membrane resistance. The first series of terms gives the summed steady-state currents through each of the segments of cleft membrane (see Fig. 12). The second series of summed terms represents transient currents through cleft membrane segments with time constants τ_n. Using the standard parameters, the above equations show that $\tau_1 = 1.5$ ms, $\tau_3 = 0.18$ ms, and $\tau_5 = 0.06$ ms. The small size of L_{in} and τ_n for $n \geq 3$ means that these higher terms can be dropped for $t \geq 0.75$ ms. It is easy to show (see Appendix) that the remaining terms on the right side of Eq. 39 describe the behavior of a "lumped" circuit (Falk and Fatt, 1964) composed of a resistor (R) and capacitor (C) in parallel with a series arrangement of a resistor (R_s) and capacitor (C_s). Eq. 37 or 39 and the values of R_m and C_m extracted from the d.c. analysis can be used to predict the lumped circuit elements corresponding to the pie model (Fig. 1 *a*) of a 100-μm strand; a similar calculation gives the lumped parameters which describe the large time behavior of the hexagonal model in Fig. 1 *b*. The results are: $R = 1.77$ and 2.21 kΩcm^2, $C = 2.86$ and 2.86 μF/cm^2, $R_s = 207$ and 143 Ωcm^2, and $C_s = 7.2$ and 5.5 μF/cm^2, respectively. These predictions, which were made without any free parameters, compare well with the values measured by Fozzard (1966): $R = 2.62$ kΩcm^2, $C = 2.4$ μF/cm^2, $R_s = 298$ Ωcm^2, $C_s = 7.0$ μF/cm^2. These predictions correspond to a time constant of 1.5 and 0.8 ms for the first segment of cleft membrane in the two models. A similar calculation of the pie model's time constant by Schoenberg et al. (1975) gave 1.7 ms. These numbers are to be compared with the measured time constant of 2.1 ms (Fozzard, 1966; Colatsky and Tsien, 1979).

Phase Angle and Impedance Measurements

One of the most powerful methods to provide a full description of the linear electrical properties of the Purkinje strand is phase angle and impedance measurement as used for study of skeletal muscle. Consider an experiment of the following type: an electrode at $x = 0$ passes an alternating current equal to $I_M e^{i\omega t}$ into a "semi-infinite" Purkinje strand; ω is $2\pi v$. Another electrode records V at position x; x is assumed to be greater than the strand diameter so that the one-dimensional cable assumption is valid. The long-term response of the voltage at x is determined by Z_x and θ_x, the magnitude of the transfer impedance and the magnitude of the phase of the transfer impedance at position x, which are

$$Z_x = Z_0 \exp\left(\frac{-xr_i \cos\theta_0}{Z_0}\right), \tag{40a}$$

$$\theta_x = \theta_0 + \frac{xr_i \sin\theta_0}{Z_0}, \tag{40b}$$

$$Z_0 = (r_i R_m)^{1/2}[1 + (R_m C_m \omega)^2]^{-1/4}[(L_e\phi_e^2 + L_i\phi_i^2 F_R)^2 + (L_i\phi_i^2 F_I)^2]^{-1/4} \tag{40c}$$

$$\theta_0 = \frac{1}{2}\tan^{-1}(R_m C_m \omega) + \frac{1}{2}\tan^{-1}\left(\frac{L_i\phi_i^2 F_I}{L_e\phi_e^2 + L_i\phi_i^2 F_R}\right), \tag{40d}$$

and

$$F(i\omega) = F_R + iF_I, \tag{40e}$$

where θ_0 is the phase angle of the characteristic admittance and F_R and F_I are the real and imaginary parts of F at $p = i\omega$. The voltage response to a current of frequency ν can now be found by substituting F for any model. For this purpose we can either use the closed form of F or the equivalent series. For example, F for the model of Fig. 1 *a* can be found from Eq. 37:

$$F_R = \frac{wR_m}{L^2R_e} \sum_{n=\text{odd}\geq 1} \frac{a_n}{a_n^2 + (R_mC_m\omega)^2}$$

$$F_I = \frac{-wR_m}{L^2R_e} \sum_{n=\text{odd}\geq 1} \frac{R_mC_m\omega}{a_n^2 + (R_mC_m\omega)^2}, \tag{41}$$

where

$$a_n = 1 + \frac{n^2\pi^2wR_m}{8L^2R_e}.$$

While at low frequency the result will depend on geometric details of the cellular arrangement in the strand, at high frequency the impedance locus will be dominated by the surface and the cleft mouths. This can be made explicit mathematically by deriving the following high frequency forms of Z_0 and θ_0 that are independent of strand diameter and cleft geometry:

$$\theta_0 = \frac{\pi}{4} - \frac{1}{2}\left[1 + \frac{L_c\phi_e^2}{\phi_i}\left(\frac{R_eC_m\omega}{w}\right)^{1/2}\right]^{-1} \tag{42a}$$

$$Z_0 = \left[\frac{r_i}{\pi D\phi_e^2C_m\omega\left[1 + \frac{\phi_i}{L_c\phi_e^2}\left(\frac{w}{R_eC_m\omega}\right)^{1/2}\right]}\right]^{1/2} \tag{42b}$$

Thus, when these formulas are accurate ($\nu \geq 300$ Hz), the impedance locus is only weakly model-dependent.

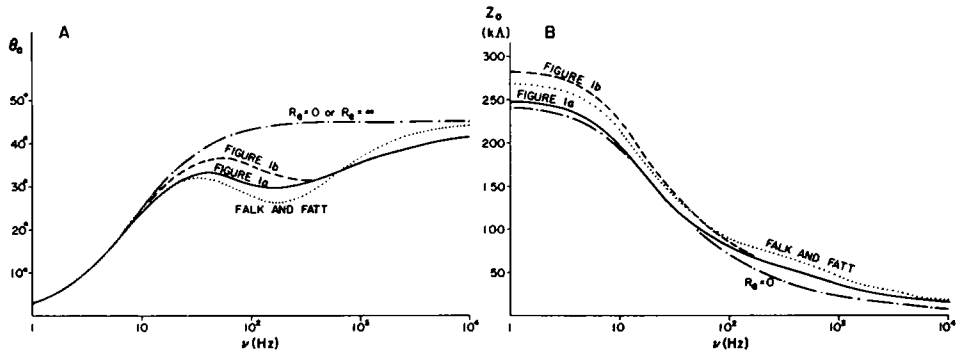

FIGURE 7 (*a*) Predictions of the 100-μm models in Fig. 1 *a* (solid line) and *b* (dashed line) for the phase angle (θ_0) of the characteristic admittance. These curves were obtained by using the electrical parameters which were extracted from the d.c. cable analysis in the text: R_m = 13 kΩcm^2, C_m = 1.5 μF/cm^2, R_i = 100 Ωcm, R_e = 50 Ωcm. The dot-dashed line is the result expected if there were no cleft effects (R_e = 0 or $R_e = \infty$). The dotted curve shows the behavior of the "lumped" Falk and Fatt model which approximates the model in Fig. 1 *a*. (*b*) Characteristic impedance (Z_0) of the same models. The dot-dashed line is the result expected in the "pie" model if there were no cleft effects (R_e = 0). The dotted curve is the "lumped" Falk and Fatt approximation to the "pie" model.

Fig. 7 *a* shows the predicted forms of θ_0 for the models in Fig. 1 *a* and *b*. R_m, C_m, R_i, and R_e were taken to have the values extracted from cable analysis. For comparison we have shown θ_0 for a fiber without cleft effects (obtained by setting $R_e = 0$ or $R_e = \infty$); the phase angle for the "lumped" Falk and Fatt circuit which approximates the pie model is obtained by keeping only the $n = 1$ term in Eq. 37 and is also exhibited in Fig. 7 *a*. Fig. 7 *b* shows the characteristic impedance (Z_0) for the same models. Notice that θ_0 is very sensitive to cleft effects, but Z_0 is not sensitive. Below 300 Hz the choice of model Fig. 1 *a* or *b* influences the phase angle, but above 300 Hz they give nearly identical results, since they are both nearly described by Eq. 42a. At very low frequencies all cleft membranes have time to conduct. It follows from Eq. 40d that θ_0 is dominated by $\frac{1}{2}\tan^{-1}(R_m C_m \omega)$, so that all curves are similar in this region, rising with a characteristic frequency $\upsilon = 1/2\pi R_m C_m \simeq 8$ Hz. The deep cleft membranes fail to conduct when the frequency exceeds the characteristic frequency of the first cleft segment: $\upsilon = 1/2\pi(1.5 \text{ ms}) \simeq 100$ Hz. This is revealed in Fig. 7 *a* when θ_0 for each model drops below the result expected for no cleft effects ($R_e = \infty$ or $R_e = 0$).

The only experimental measurements of phase angle in Purkinje strands were made by Freygang and Trautwein (1970). They measured θ_x for a small but undetermined x, selected to minimize θ_x. Qualitative comparison of Fig. 7 with the results of Freygang and Trautwein (1970) shows general agreement, with the dip of θ_o produced by the clefts occurring near 300 Hz. Fig. 8 shows how θ_0 in model 1 *a* varies with changes in R_m when C_m, R_i, and R_e are held constant. Note that the peak in θ_0 is depressed and shifted to a higher frequency as R_m is decreased. Above 100 Hz the curves converge to the high frequency behavior described by Eq. 42, which is independent of R_m. Fig. 8 of Freygang and Trautwein (1970) shows measurements of θ_x before and after a change of extracellular K^+ from 5.4 to 55.4 mM. The measured shift of θ_x resembles that predicted in our Fig. 8 when R_m decreases.

Our predictions cannot be compared quantitatively with the results of Freygang and Trautwein (1970) since they did not measure the interelectrode distance x. For example, in most of their studies θ_x was observed to exceed 45° at high frequencies. While this could result from radial and longitudinal capacitive elements in the strand's core (presumably at

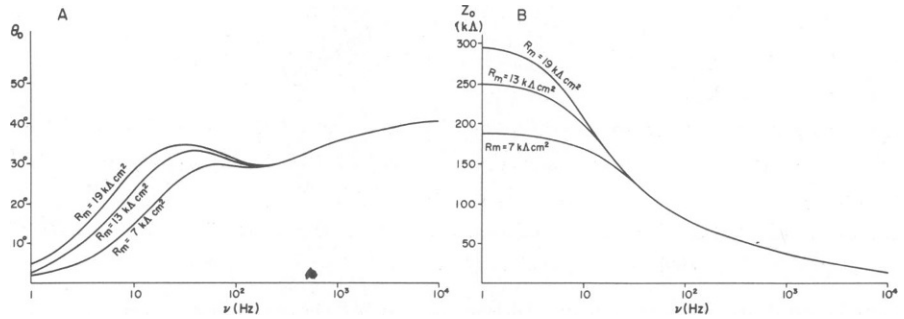

FIGURE 8 (*a*) R_m-dependence of the phase angle of the characteristic admittance for the 100-μm "pie" model in Fig. 1 *a*. These predictions are obtained by evaluating Eqs. 40d and 41 with the electrical parameters extracted from the cable analysis in the text: $R_m = 13$ kΩcm², $C_m = 1.5$ μF/cm², $R_i = 100$ Ωcm, $R_e = 50$ Ωcm; then R_m is allowed to vary between 7 and 19 kΩcm². (*b*) Characteristic impedance for the same model.

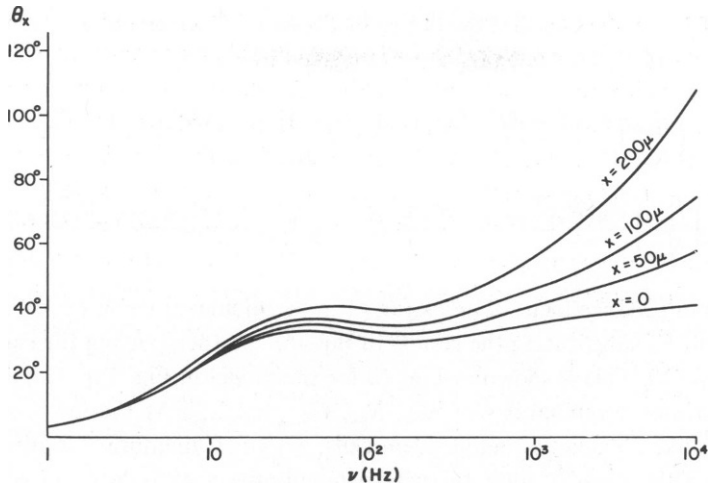

FIGURE 9 The magnitude of the phase of the transfer impedance (θ_x) for various electrode separations (x) is plotted against frequency. This has been computed for the 100-μm "pie" model in Fig. 1 *a* by combining Eqs. 40 and 41; electrical parameters were taken to have the values extracted from the cable analysis in the text: R_m = 13 kΩcm^2, C_m = 1.5 μF/cm^2, R_i = 100 Ωcm, R_e = 50 Ωcm.

intercellular junctions), these authors did not explicitly correct their results for other effects that can cause θ_x to exceed 45° in a fiber with a purely resistive core: i.e., the three-dimensional spread of current and the fact that x was non-zero (Fig. 9). The issue may be resolved by impedance locus measurements which account for these phenomena (R. Levis, personal communication). Specific analysis of longitudinal impedance by Freygang and Trautwein (1970) also showed a core reactance, reinforcing the implications of their impedance locus studies. To incorporate this property we replace R_i with $R_i\gamma(i\omega)$. γ can be written as the product of a magnitude and phase factor: $\gamma(i\omega) = |\gamma(i\omega)|e^{-2i\phi(\omega)}$. Then Eqs. 40 and 42 are modified by replacing r_i by $r_i|\gamma(i\omega)|$ and by adding ϕ to the right side of the equation for θ_0; i.e., Eq. 40d becomes

$$\theta_0 = \frac{1}{2}\tan^{-1}(R_mC_m\omega) + \frac{1}{2}\tan^{-1}\left(\frac{L_i\phi_i^2F_I}{L_e\phi_e^2 + L_i\phi_i^2F_R}\right) + \phi. \tag{43}$$

This shows that the phase of the strand's characteristic admittance will exceed 45° at high frequencies if the core has a capacitive reactance, as reported by Freygang and Trautwein (1970). The effect of ϕ will be small for $\upsilon \leq 300$ Hz.

For the above discussion it has been assumed that R_m and C_m are the same for surface and cleft membrane. If the membrane admittances are not the same, then

$$y_m = L_e\phi_e^2\,Y_e + L_i\phi_i^2Y_iF, \tag{44}$$

where $Y_e = 1/R_{me} + C_{me}p$ and $Y_i = 1/R_{mi} + C_{mi}p$. F depends on λ_c, which is a function of Y_i, i.e. $\lambda_c = (w/2R_eY_i)^{1/2}$. Eq. 44 can be rewritten as

$$y_m = Y_e(L_e\phi_e^2 + L_i\phi_i^2\tilde{F}), \tag{45}$$

where $\tilde{F} = Y_i F/Y_e$. It follows that the impedance locus is described by Eq. 40 with R_m and C_m replaced by R_{me} and C_{me} and with F_R and F_I replaced by $\tilde{F}_R$ and $\tilde{F}_I$:

$$\tilde{F}_R = \left(\frac{R_{me}}{R_{mi}}\right) \frac{F_R[1 + (R_{mi}C_{mi}\omega)(R_{me}C_{me}\omega)] - F_I[R_{mi}C_{mi}\omega - R_{me}C_{me}\omega]}{1 + (R_{me}C_{me}\omega)^2},$$

$$\tilde{F}_I = \left(\frac{R_{me}}{R_{mi}}\right) \frac{F_R[R_{mi}C_{mi}\omega - R_{me}C_{me}\omega] + F_I[1 + (R_{mi}C_{mi}\omega)(R_{me}C_{me}\omega)]}{1 + (R_{me}C_{me}\omega)^2}, \quad (46)$$

Therefore, the impedance locus of any strand can be calculated using Eq. 14b and Table I to compute F_R and F_I, substituting the results in Eq. 46, and then putting the expressions for $\tilde{F}_R$ and $\tilde{F}_I$ into Eqs. 40. This is shown in Fig. 10 for the model in Fig. 1 *a*. The phase angle θ_0 is graphed for various combinations of R_{me}, R_{mi}, C_{me}, and C_{mi}. At the low frequency end the strand behaves like a packet of independent cells, with cleft membrane in direct contact with the bath. Since the ratio of cleft to surface membrane area is large ($L_i\phi_i^2/L_e\phi_e^2 \simeq 4$), the behavior of θ_0 is dominated by the time constant of the cleft membrane. At high frequencies ($\upsilon \geq 300$ Hz) the phase angle is described by the universal formula in Eq. 42, modified for the differing admittances of the surface and cleft membranes:

$$\theta_0 = \frac{\pi}{4} - \frac{1}{2}\left[1 + \frac{L_c\phi_e^2}{\phi_i}\left(\frac{R_e C_{me}^2 \omega}{C_{mi} w}\right)^{1/2}\right]^{-1}. \quad (47)$$

This explains why the high frequency phase angle in Fig. 10 is independent of the values of surface and cleft resistivity. It also shows why the phase angle is depressed by increases in C_{mi}, but enhanced by increases in C_{me}.

The phase angle is also sensitive to the value of the cleft resistivity R_e. Fig. 11 shows the effect on θ_0 and Z_0 of raising R_e in the model 1 *a*. Recall that low frequency values of θ_0 reflect the properties of the deep cleft membranes. Therefore accurate measurements of θ_0 at low frequencies will reveal the resistivity of the solution in the deep cleft spaces. For example, comparison of Fig. 11 with the data of Freygang and Trautwein (1970) indicates that R_e in the clefts is probably close to that of Tyrode solution.

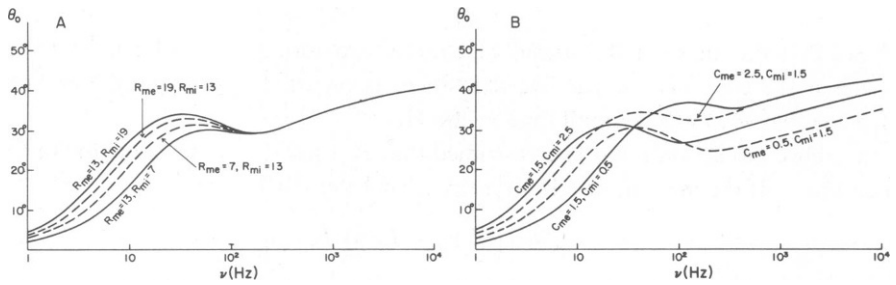

FIGURE 10 The phase angle of the characteristic admittance for fibers in which the external and internal unit membranes have different resistivities (R_{me}, R_{mi}) and capacities (C_{me}, C_{mi}). These graphs were calculated for the "pie" model (Fig. 1 *a*) as outlined in the text. The fundamental electrical parameters were taken from cable analysis: R_i = 100 Ωcm, R_e = 50 Ωcm, $C_{me} = C_{mi}$ = 1.5 μF/cm² in *a*, and $R_{me} = R_{mi}$ = 13 kΩcm² in *b*.

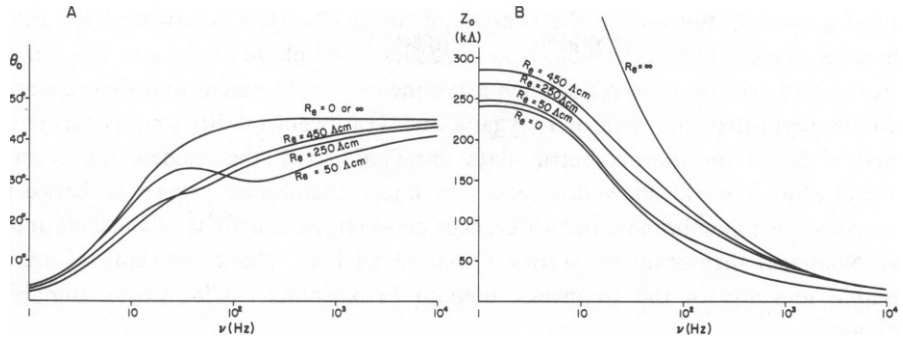

FIGURE 11 *a* and *b* show how θ_0 and Z_0 in the 100-μm "pie" model (Fig. 1 *a*) change as the resistivity of the cleft medium is varied. R_m, C_m, and R_i are held fixed at the values extracted from the cable analysis in the text: R_m = 13 kΩcm^2, C_m = 1.5 μF/cm^2, R_i = 100 Ωcm.

DISCUSSION

A model is developed for a multicellular strand of cardiac cells like the Purkinje strand, using the morphometric data of Mobley and Page (1972) and Hellam and Studt (1974 *a*). This model contains clefts, defining a limited extracellular space. Electrical measurements justify the notion of tight electrotonic coupling of cells in the transverse and longitudinal planes, with intercalated disks interpreted as junctions of low resistance and possibly significant capacitance (Freygang and Trautwein, 1970). Hellam and Studt (1974 *a*) and Schoenberg et al. (1975) suggested a pie model of a small strand in which the cells are triangular in shape. Their model provided a good fit to ramp voltage and cable analysis experiments. In those papers the influence of alternative cell arrangements was not considered, strands of large diameter were not described mathematically, and the form of the equations was not suitable for modeling of impedance locus data.

In this report the solution of the differential equations describing strand admittance was achieved analytically, leading to a description of how the experimentally measured quantities depend on the detailed geometrical structure and the unit electrical properties. Comparison of the model with collected data from many cable analysis and voltage step experiments suggests that some geometrical factors are of great importance. The surface to volume ratio of the strand (number of cells in the strand), the membrane folding factors, and the cleft width play critical roles in the strand behavior. Certain aspects of the model that were fixed for convenient analysis are not important determinants of strand behavior. For example, all cell sides need not be the same length, if the average length is large relative to width. The number of clefts at a junction may vary between three and six, clefts need not have a constant width, and the strand does not need to have a constant diameter, as long as the measurements are made over a length much greater than the strand diameter. More detailed tests of the model will depend on a comparison between the precise geometrical description and electrical properties of individual strands.

Equations were developed to describe the high frequency domain where strand behavior is largely independent of internal structure. The accuracy of these equations depends on the shortness of the cleft length constant, relative to the length of a cell side, at frequencies above 300 Hz. They can be tested by experimental alteration of conduction velocity.

The most powerful approach to the analysis of linear electrical behavior of the Purkinje strand is measurement of the characteristic impedance and phase angle, and this analytical model provides a basis for interpreting such experiments. To the extent that their experimental conditions permitted, the data of Freygang and Trautwein (1970) were consistent with these models based on morphometric data. Predictions of the models indicated that experimental studies could show differences in linear membrane properties between the surface and the cleft membranes, and differences between the resistivity of the cleft and bath solutions. Nonlinear membrane properties of muscle, such as "charge movement," may also be amenable to study in the frequency domain (Takashima, 1978; Levin, unpublished observations).

APPENDIX

Equivalent Circuits

The admittance of the pie model (Fig. 1 *a*) is described by the closed form obtained from Eqs. 14a, 14b, and Table I. On the other hand, Cauchy's theorem can be used to express the same admittance as the infinite series in Eq. 37. The series representation has the following simple intuitive interpretation. The first term $L_e\phi_e^2 Y$ is the admittance of the folded external membrane. The n^{th} term in the infinite series is just the admittance of a segment of laminated membrane which is L_{in} in length and which consists of a layer with specific admittance Y in series with a purely resistive layer of specific resistivity R_{sn}. Notice that

$$\sum_{n\text{-odd}\geq 1} \frac{1}{n^2} = \frac{\pi^2}{8},$$

so that the sum of all L_{in} is just L_i. Therefore, the infinite series in Eq. 37 represents the internal membrane (with cleft effects included) as the terraced array of laminated segments in Fig. 12. The first

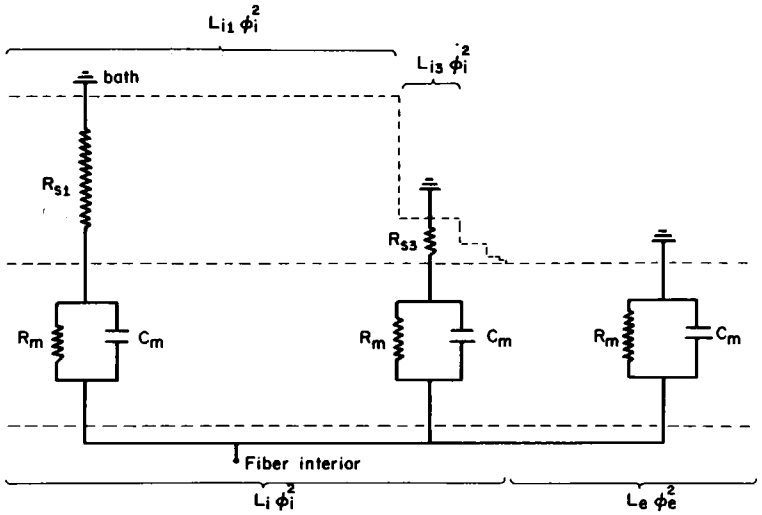

FIGURE 12 The electrical circuit which is exactly equivalent to the closed form expression for y_m for the model in Fig. 1 *a*. R_m and C_m are the actual unit membrane resistivity and capacitance; Eq. 37 gives R_{sn} and L_{in} in terms of microscopic parameters of the clefts.

segment of the internal membrane has length $L_{i1} \simeq 0.8\ L_i$ and represents predominantly deep internal membrane which is connected to the bath by a relatively large resistance, $R_{s1} \simeq 0.8\ (L^2R_e/w)$. The next segment is much shorter ($L_{i3} \simeq 0.1\ L_i$); it represents a stretch of internal membrane which is near the cleft mouths and which is connected to the bath by a small resistance, $R_{s3} \simeq 0.1\ (L^2R_e/w)$. Higher terms in the series correspond to even shorter segments which are even more superficially located in the fiber.

The circuit in Fig. 12 is distributed version of the "lumped" circuit discussed by Falk and Fatt (1964). To see this, consider the circuit obtained from Fig. 12 by omitting the terraces with $n \geq 3$. It is not hard to show that the resulting circuit is electrically equivalent to the Falk and Fatt circuit constructed from a resistor and capacitor in parallel with a series arrangement of another resistor and capacitor. Therefore, the complete circuit in Fig. 12, which emerges naturally from the differential equations of electrical conduction, is a distributed Falk and Fatt model. A similar calculation shows that the analytical solutions for the other models in Fig. 1 are also equivalent to circuits like Fig. 12, although the values of the electrical components (R_{sn}) and distribution parameters (L_{in}) are model-dependent.

We are grateful to M. Schoenberg for helpful discussions. This work was supported by U.S. Public Health Service grant HL-20592.

Received for publication 30 June 1980 and in revised form 10 September 1980.

REFERENCES

ADRIAN, R. H, and W. ALMERS. 1974. Membrane capacity measurements on frog skeletal muscle in media of low ionic content. *J. Physiol. (Lond.).* **237**:573–606.

ADRIAN, R. H., W. K. CHANDLER, and A. L. HODGKIN. 1969. The kinetics of mechanical activation in frog muscle. *J. Physiol. (Lond.).* **204**:207–230.

COLATSKY, T. J., and R. W. TSIEN. 1979. Electrical properties associated with wide intercellular clefts in rabbit Purkinje fibers. *J. Physiol. (Lond.).* **290**:277–294.

DEMELLO, W. C. 1975. Effect of intracellular injection of calcium and strontium on cell communication in heart. *J. Physiol. (Lond.).* **250**:231–245.

EISENBERG, R. S., and E. A. JOHNSON. 1970. Three-dimensional electrical field problems in physiology. *Prog. Biophys. Mol. Biol.* **20**:1–65.

FALK, G., and P. FATT. 1964. Linear electrical properties of striated muscle fibres observed with intracellular electrodes. *Proc. R. Soc. Lond. B. Biol. Sci.* **160**:69–123.

FOZZARD, H. A. 1966. Membrane capacity of the cardiac Purkinje fiber. *J. Physiol. (Lond.).* **182**:255–267.

FOZZARD, H. A., and M. SCHOENBERG. 1972. Strength-duration curves in cardiac Purkinje fibers: effects of liminal length and charge distribution. *J. Physiol. (Lond.).* **226**:593–618.

FREYGANG, W. H., and W. TRAUTWEIN. 1970. The structural implications of linear electrical properties of cardiac Purkinje strands. *J. Gen. Physiol.* **55**:524–547.

HELLAM, D. C., and J. W. STUDT. 1974 *a*. A core-conductor model of the cardiac Purkinje fibre based on structural analysis. *J. Physiol. (Lond.).* **243**:637–660.

HELLAM, D. C., and J. W. STUDT. 1974 *b*. Linear analysis of membrane conductance and capacitance in cardiac Purkinje fibers. *J. Physiol. (Lond.).* **243**:661–694.

HODGKIN, A. L., and W. A. S. RUSHTON. 1946. The electrical constants of a crustacean nerve fibre. *Proc. R. Soc. Lond B Biol. Sci.* **133**:444–479.

HUNTER, P. J., P. A. MCNAUGHTEN, and D. NOBLE. 1975. Analytical models of propagation in excitable cells. *Prog. Biophys. Mol. Biol.* **30**:99–144.

MATHIAS, R. T., R. S. EISENBERG, and R. VALDIOSERA. 1977. Electrical properties of frog skeletal muscle fibers interpreted with a mesh model of the tubular system. *Biophys. J.* **117**:57–93.

MCALLISTER, R. E., D. NOBLE, and R. W. TSIEN. 1975. Reconstruction of the electrical activity of cardiac Purkinje fibres. *J. Physiol. (Lond.).* **251**:1–59.

MOBLEY, B. A., and E. PAGE. 1972. The surface area of sheep cardiac Purkinje fibres. *J. Physiol. (Lond.).* **220**:547–563.

SCHNEIDER, M. F. 1970. Linear electrical properties of the transverse tubules and surface membranes of skeletal muscle fibers. *J. Gen. Physiol.* **56**:640–671.

SCHNEIDER, M. F., and W. K. CHANDLER. 1976. Effects of membrane potential on the capacitance of skeletal muscle fibers. *J. Gen. Physiol.* **67**:125–163.

SCHOENBERG, M., G. DOMINGUEZ, and H. A. FOZZARD. 1975. Effect of diameter on membrane capacity and conductance of sheep cardiac Purkinje fibers. *J. Gen. Physiol.* **65**:441–458.

SCHOENBERG, M., and H. A. FOZZARD. 1979. The influence of intercellular clefts on electrical properties of sheep cardiac Purkinje fibers. *Biophys. J.* **25**:217–234.

SOMMER, J. R., and E. A. JOHNSON. 1968. Cardiac muscle: a comparative study of Purkinje fibers and ventricular fibers. *J. Cell. Biol.* **36**:497–526.

TAKASHIMA, S. 1978. Frequency domain analysis of asymmetry currents in squid axon membrane. *Biophys. J.* **22**:115–119.

TASAKI, I., and S. HAGIWARA. 1957. Capacity of muscle fiber membrane. *Am. J. Physiol.* **188**:423–429.

VALDIOSERA, R., C. CLAUSEN, and R. S. EISENBERG. 1974. Circuit models of the passive electrical properties of frog skeletal muscle fibers. *J. Gen. Physiol.* **63**:432–459.

WEIDMANN, S. 1952. The electrical constants of Purkinje fibres. *J. Physiol. (Lond.).* **118**:348–360.

WEINGART, R. 1977. The actions of ouabain on intercellular coupling and conduction velocity in mammalian ventricular muscle. *J. Physiol. (Lond.).* **264**:341–365.